

中国激光

高频宽带分布相参微波光子成像雷达研究

邢云路, 李尚远, 薛晓晓, 郑小平^{*}

清华大学电子工程系北京信息科学与技术国家研究中心, 北京 100084

摘要 高频宽带分布相参微波光子成像雷达具有速度分辨率高、距离分辨率高、角度分辨率高、信噪比高等优点, 是高精度成像雷达的一个发展方向。其核心功能模块包括: 微波光子信号产生、光学分数域接收前端及高精度光纤时频同步环网。对上述三个关键模块的国内外发展现状进行了简要回顾, 重点介绍了我国在国家自然科学基金重大项目支持下, 在动态可重构波形产生、光学分数域接收前端、高精度时频同步环网等方面取得的成果, 以及基于这些成果搭建的基于微波光子学原理的 X 波段分布相参宽带成像雷达实验系统以及阶段性的实验结果。

关键词 微波光子学; 分布式相参; 雷达; 光纤时频同步网; 分数傅里叶变换

中图分类号 TN29 文献标志码 A

doi: 10.3788/CJL202148.1517003

1 引言

分布相参雷达利用多个分离的天线孔径进行联合探测, 以多部雷达相参收发的方式实现高信噪比(SNR)接收^[1-4]。分布相参雷达往往由 1 个中心控制站和 N 部单元雷达构成, 通过收发相参, 可将回波信噪比提升 N^3 倍。分布式相参结合高频宽带, 在目标探测的速度分辨率、径向分辨率、横向分辨率等方面有着巨大的优势, 有望在应对诸如弹道导弹、高速隐身飞机、无人机等低雷达截面积、高机动或低空慢速飞行的目标的威胁方面发挥重要作用, 因此, 引起了国内外科研人员的广泛关注。美国麻省理工学院林肯实验室、我国多个研究单位在暗室或外场开展了一系列相参合成实验, 取得了 C/P/X/Ka 等波段分布相参融合的成果, 并获得了一定的信噪比增益^[1-8]。然而基于传统电子学构建高频宽带分布相参成像雷达时存在不少瓶颈问题, 其中较为突出的有: 宽带信号的产生^[9-10] 和大距离范围内高精度时频同步^[11-12]。受制于电子瓶颈, 已报道的分布相参雷达系统带宽普遍小于 2 GHz, 距离分辨率较低; 受制于电缆的传输损耗, 以及时频同步精度, 这些系统均未能实现大距离范围内分布。

微波光子技术是解决上述瓶颈问题的一种可行途径^[13]。得益于光子器件带宽大、幅频响应平坦、并行处理能力强等优点, 微波光子技术可直接产生和处理高频宽带雷达信号^[14-16]。光纤低损耗、大带宽的优势也有利于传递时频同步信号、构建高精度光纤时频同步网^[17]。

我国在国家自然科学基金委的支持下, 实现了基于微波光子学原理的 X 波段、带宽为 4 GHz 的 2 发 2 收分布相参宽带成像雷达实验系统, 获得了厘米量级的成像分辨率。本文在回顾微波光子信号产生、光学分数域(FrFD)接收前端及高精度光纤时频同步环网三个关键模块现状的基础上, 重点介绍我国在基于微波光子学分布式相参宽带雷达的核心技术与阶段性实验结果。

2 关键技术简介

2.1 分布相参微波光子成像雷达总体架构与工作流程

所提出的分布相参微波光子成像雷达系统总体架构如图 1 所示, 中心控制站(CCS)和 N 部单元雷达(UR1, UR2, …, URN)由光纤环形时频同步网(OTFSN)连接。中心控制站将原子钟(Rb)产生的

收稿日期: 2021-03-02; 修回日期: 2021-05-06; 录用日期: 2021-05-17

基金项目: 国家自然科学基金(61690191, 61690192)

通信作者: *xpzheng@mail.tsinghua.edu.cn

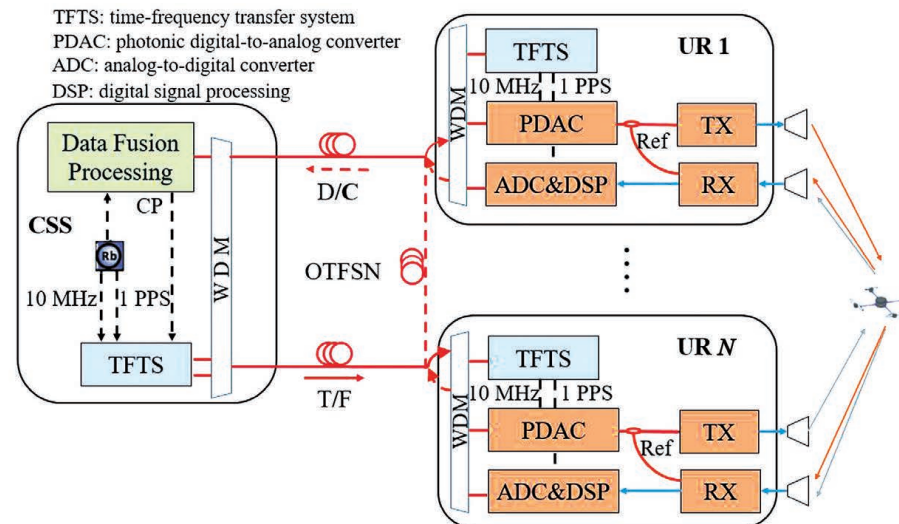


图 1 分布相参微波光子成像雷达总体架构

Fig. 1 Overall framework of the distributed coherent-aperture microwave photonic imaging radar

时频参考信号(T/F)由OTFSN传输到各单元雷达,以触发各单元雷达的收发机。中心站和单元雷达间的数据和控制信号(D/C)由光纤网络交换。

分布式相参的基本工作流程为:1)发现目标后,各单元雷达进行相参估计。通过发射彼此正交的宽带波形,测量各雷达单元和目标的延时。2)基于测量结果调整各个单元雷达与目标之间的信号传输时间,使其相同,达到相参的要求。3)发射宽带线性调频波(LFMW),进行全相参成像。此时,雷达可获得 N^3 倍信噪比增益。

2.2 动态可重构波形产生

直接数字频率合成技术可产生动态可重构的雷达波形,但该方案难以产生带宽大于2 GHz的雷达信号,由此限制了距离分辨率。为了突破这一瓶颈,研究人员提出了多种基于微波光子技术的雷达信号产生方法:1)光频时映射法。该方法先将光脉冲发生器产生的宽谱信号进行频谱整形,然后将频谱通过色散元件映射到时域,最后通过光电探测器检测出时域包络。该方案产生的信号时宽较小,往往只有几纳秒,限制了其使用^[18-19]。2)微波光子倍频法。该方法将电域产生的窄带信号调制到光域,然后进行高次倍频,产生宽带信号。这种方法可以方便地产生宽带线性调频波,但产生其他类型的波形相对困难^[20-21]。3)光注入半导体激光器法。通过改变外注入光调制的电信号,动态控制注入激光器的光强度,从而实现对所产生的微波信号瞬时频率的控制。这种方法产生的微波信号,其相位相干性不理想^[22-24]。4)相位调制与外差法。该方法通过相位调制两个相位相关的光波,使相位差为所需相位,然后

拍频得到所需要的微波信号。该方案结构比较简单,但信号的时间带宽积较小^[25-26]。

分布相参雷达需要产生多通道宽带正交波形用于相参参数估计,产生宽带线性调频波用于相参成像。这给信号产生提出了新要求:宽带、动态可重构、相参。为满足上述需求,提出如图2所示的宽带动态可重构波形产生方案,该方案由清华大学早期研制的光子数模转换(PDAC)^[27]和相位编码模块两部分组成。PDAC产生宽带线性调频波。相位编码模块由双输出马赫-曾德尔调制器(DOMZM)和平衡探测器(BPD)构成。

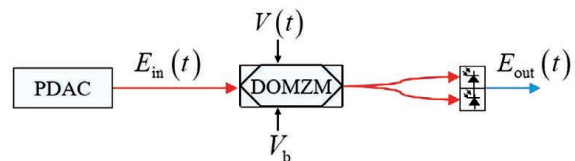


图 2 动态可重构波形产生模块

Fig. 2 Configuration of the dynamic reconfigurable waveform generation module

设PDAC产生的波形为 $E_{in}(t)$,控制信号为 $V(t)$,DOMZM半波电压为 V_π ,工作点设置电压为 V_b ,则当 $V_b=V_\pi/2$ 时,输出波形为

$$E_{out}(t) = \begin{cases} 2|E_{in}(t)|^2, & V(t) = +1 \text{ V} \\ -2|E_{in}(t)|^2, & V(t) = -1 \text{ V} \end{cases} \quad (1)$$

可见,当控制信号在±1 V间跳变时,动态可重构波形产生模块输出相位正交的PDAC波形。当 $V_b=0$ V且 $V(t)=0$ V时, $E_{out}(t)=2|E_{in}(t)|^2$ 。

用该装置产生了两路8.5~11.5 GHz,脉冲宽度为8 μs,重复周期为10 μs的信号。正交相位编

码是码率为 0.5 Gbit/s 的 12 位 m 序列, 截取前 4000 位作为第 1 路正交波形的编码序列(记为 y_1), 该序列向右循环移位 100 位作为第 2 路正交波形的编码序列(记为 y_2)。两路波形分别由示波器

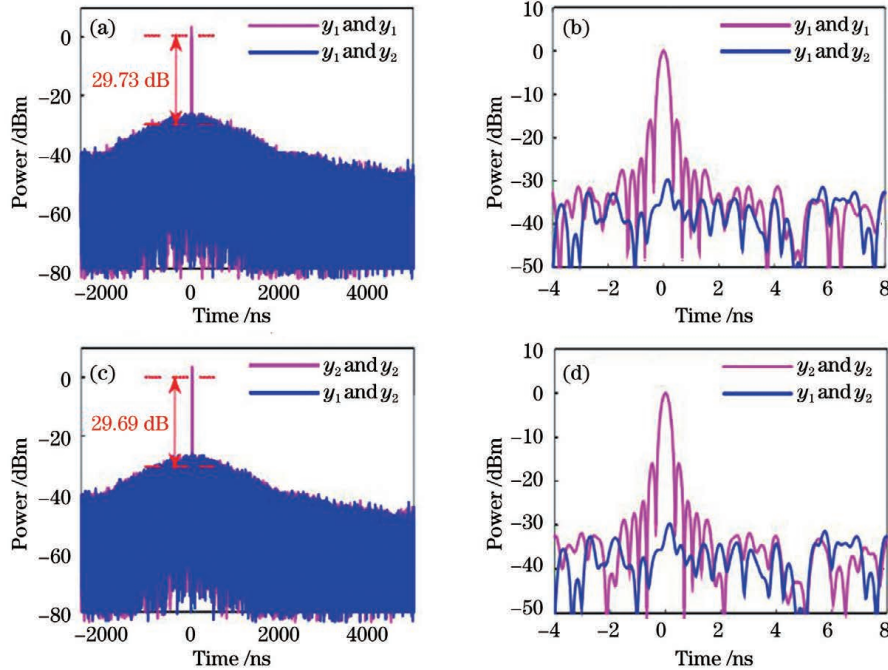


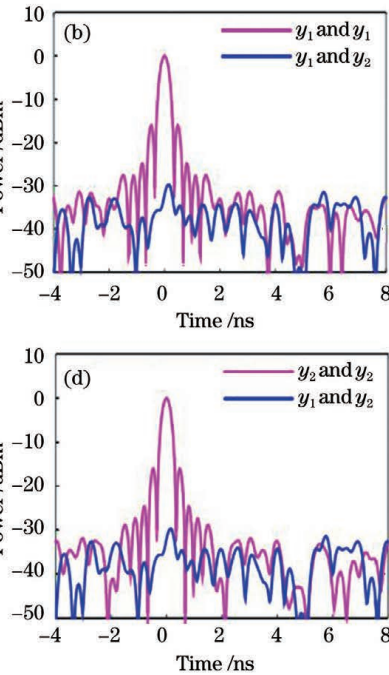
图 3 波形正交性结果^[28]; (a) y_1 的自相关与 y_1 、 y_2 的互相关结果; (b) 图 3(a) 中主瓣附近的细节图; (c) y_2 的自相关与 y_1 、 y_2 的互相关结果; (d) 图 3(c) 中主瓣附近的细节图

Fig. 3 Results of waveform orthogonality^[28]. (a) Auto-correlation of y_1 and cross-correlation of y_1 and y_2 ; (b) detail near the main lobe in Fig. 3(a); (c) auto-correlation of y_2 and cross-correlation of y_1 and y_2 ; (d) detail near the main lobe in Fig. 3(c)

2.3 光学分数域接收前端

目前, 高频宽带雷达波形光学接收方案主要包括光子模数转换(ADC)直接采样、光子信道化接收、光子辅助压缩感知以及微波光子去斜接收。在光子 ADC 直接采样接收方案中, 光子 ADC 对宽带雷达回波进行采样与下变频等处理, 然后经过电子 ADC 采样, 并在数字域进行处理, 得到目标信息^[29-30]。对于宽带信号, 上述方案的后端处理数据量很大, 难以实现实时成像。在光子信道化接收方案中, 通过将宽带信号在模拟域^[31]或数字域^[32]“切割”为多个窄带信号并分别处理, 从而得到接收回波信息。该方案的通道错配会影响信号的重构效果^[33]。光子辅助压缩感知接收方案可充分发掘雷达回波的稀疏性, 其将冗余信息压缩, 缓解了数据量大的问题^[34-35]。但当雷达回波信噪比较低时, 稀疏恢复的性能较差^[33]。微波光子去斜方案将接收到的回波与本地雷达信号差拍得到窄带信号, 从中推算出目标距离。该方案将高频宽带信号转化为低频窄带信号, 有效地降低了后端 ADC 采样率, 减少了

(OSC)采样与数字信号处理器(DSP)处理, 结果如图 3 所示: y_1 的自相关比二者互相关的峰值功率高 29.73 dB; y_2 的自相关比二者互相关的峰值功率高 29.69 dB。实验和理论预期吻合。



信号处理的数据量, 受到广泛关注^[36-37]。当前微波光子去斜接收主要应用在单目标成像场景中, 而对实际场景中数目、位置未知的多非合作目标进行探测时, 往往会出现鬼像。为解决这个问题, 研究人员提出了一种基于平衡 I/Q 探测的微波光子去斜方案, 该方案可消除由不同延时回波互相差拍产生的鬼像, 但是其复杂性较高^[38]。随后清华大学的研究学者们提出了一种结构更为简单的、基于光学分数域原理的接收前端。

微波光子成像雷达中光电转换的本质是一种二阶非线性运算, 雷达接收到的目标相参回波经过非线性运算, 将产生一种固有的非线性干扰, 形成鬼像。由于雷达信号是一种时频二维信号, 故 Han 等^[39]提出利用分数域非线性光学调控的思想来解决该问题。接收前端的原理结构及其分数域非线性调控的过程如图 4 所示, 接收前端的输出可表示为

$$F_a(f') = \int S_r(t) S_o^*(t) \exp(-j2\pi f' t) dt \propto \delta[2\pi(f' - k\tau)], \quad (2)$$

式中: $S_r(t)$ 为接收信号, $S_o(t)$ 为本地信号, f' 为分步阶频率, τ 为回波延时, $\delta(\cdot)$ 为 Dirac 函数, 即冲激函数, k 为发射信号的啁啾率。 $S_o(t)$ 作为旋转基旋转接收信号的时频面, 其旋转角度 α 满足 $\cot \alpha = -2\pi k$ 。

回波 LFMW 被投影到分数域, 其分数域频谱 $F_a(f')$ 为冲激函数。这个过程将分数域重叠信号转换为分离信号。当 $S_r(t)$ 包含多个目标回波时, 每个回波充当伪旋转基旋转其他回波的时频面, 最终各个回波在新的时频域上形成冲激函数, 相互分离。这些分离信号间的二阶非线性干扰, 可用双臂平行调制器(DPMZM)来处理。由此证明: 当双臂

平行调制器静态工作点被控制在 $\phi_1 = \pi/4$, $\phi_2 = \pi/2$, $\phi_3 = 0$ 时, 图 4 所示的结构在理论上可完全抑制回波间的二阶非线性, 且该组静态工作点参数不受线性调频波参数的影响, 具有普适性^[39]。在实际使用中, 为了得到较高的鬼像抑制比, 需要对三个工作点进行准确、稳定的控制。现有的基于导频法的偏置点控制方案可满足这一需求^[40]。

验证性实验如图 5 所示。实验采用 8~12 GHz 的 LFMW, 对双目标进行探测, 用实时示波器(DSO)采集数据。

首先用传统的基于 DPMZM 的去斜方案^[36] 对如图 6(a)所示的双目标进行探测。将 MZM1 和

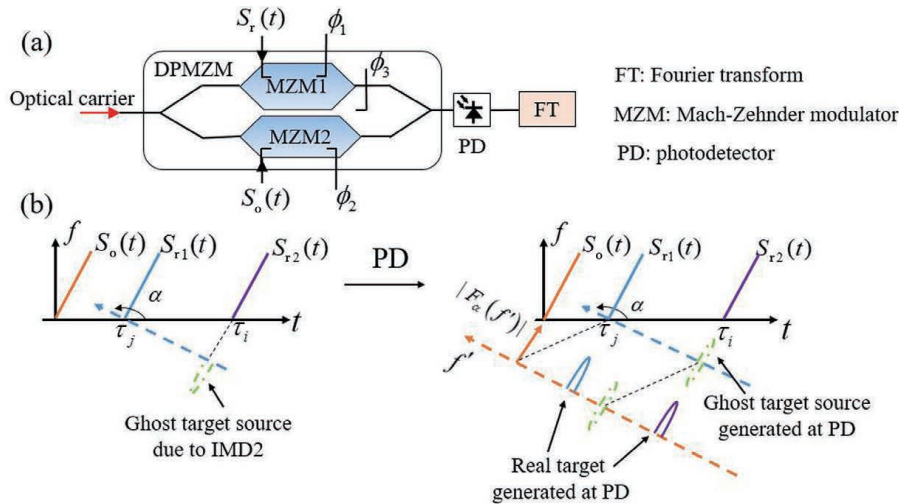


图 4 光学分数域接收前端结构及原理。(a)光学分数域接收前端基本结构;(b)鬼像消除原理

Fig. 4 Schematic diagram and principle of the proposed optical FrFD receiver front-end. (a) Schematic diagram of the optical FrFD receiver front-end; (b) principle of ghost target elimination

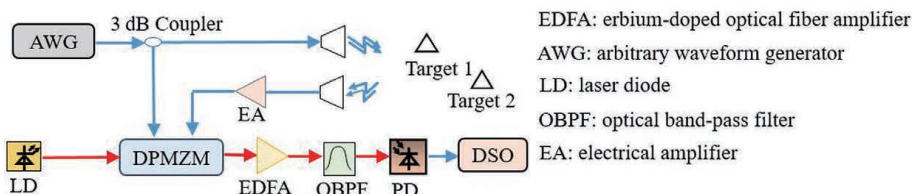


图 5 光学分数域接收前端实验结构

Fig. 5 Experimental setup of optical FrFD receiver front-end

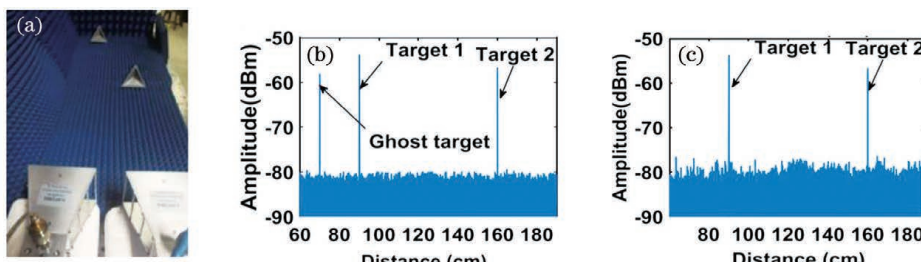


图 6 多目标探测实验结果^[39]。(a)两角反射器放置在不同位置;(b)未经过鬼像消除结果;(c)经过鬼像消除结果

Fig. 6 Experimental results of multiple targets detection^[39]. (a) Two corner reflectors placed at different distances; (b) results without ghost target elimination; (c) results with ghost target elimination

MZM2 偏置在最小传输点, MZM3 偏置在最大传输点, 结果如图 6(b)所示, 出现了假目标。用光学分数域接收前端接收, 假目标被消除, 如图 6(c)所示。

2.4 高精度光纤时频同步环网

为了获得高信噪比增益, 各单元雷达需要保证时间和频率同步。基于微波光子学原理的时频同步技术可在大距离范围内对多个单元雷达实现高精度时频同步。

微波光子频率同步技术可主要分为主动相位波动补偿技术和被动相位波动补偿技术。主动补偿技术基本原理为: 将微波参考信号在同一光纤链路中经往返传输和鉴相后得到包含光纤相位波动的误差信号, 利用该信号反馈控制可调光延迟线改变光程长度^[41-42], 或反馈控制移相器改变传输信号的相位^[43-44], 也可通过声光调制器对光载微波信号进行频率调控, 从而实现对光纤时延波动的补偿^[45]。被动补偿技术通过产生相位共轭信号并以混频的方式自适应消除光纤引入的相位波动, 补偿范围大, 结构简单^[46-48]。

光纤时间传递当前主要有链路波动补偿和双向时间传递两种实现方式。链路波动补偿方案通过精确测量信号往返传输时延, 反馈控制可调延时线, 补偿光纤延时波动, 并基于测量时延校准时差, 实现时间同步^[49-50]。然而该方案的补偿范围受限于补偿器件。双向时间传递方案则是使本地站和远端站同时经光纤链路传递时间信号, 测得双向传输时延, 通过

时间差调整时钟实现时间同步。然而该方案往往需要载波处理器或编解码器, 增加了系统的复杂性^[51-52]。

针对分布相参雷达高精度时频同步的需求, 本课题组提出一种基于微波光子信号处理的微波相位共轭技术, 利用相位共轭实现了环网的频率同步^[53]; 在此基础上, 基于时-频转换测量技术, 提出了一种双向时间同步技术^[54]。最终, 两个技术合二为一, 实现了时频同步环网^[55]。由于环网具备 50 ms 保护能力, 因此该同步方式具有很好的生存能力。

基于相位共轭原理的频率同步网如图 7 所示。本地站微波源产生频率为 ω_r 、初始相位为 φ_r 的参考信号, 表达式为 $V_1 = \cos(\omega_r t + \varphi_r)$ 。MZM1 通过载波抑制双边带调制(CS-DSB)参考信号, 并将其分为两路, 一路通过单模光纤 SMF1 传至远端站, 作为前向传输光信号, 表达式为

$$E_1 \propto \exp[j\omega_c(t - \tau_1)] \cdot \cos(\omega_r t - \varphi_1 + \varphi_r), \quad (3)$$

式中, τ_1 和 φ_1 分别为 SMF1 引入的时延和相移, ω_c 为载波频率。另一路通过光电探测器 PD1 转换得到参考信号的二倍频信号 $V_2 = \cos[2(\omega_r t + \varphi_r)]$ 。将 N 个远端站连接到环形光纤链路中, 频率信号经 $N+1$ 段单模光纤传输所积累的相位波动为 $\varphi_s = \varphi_1 + \varphi_2 + \dots + \varphi_{N+1} = \omega_r \tau_s$, 其中 φ_k 为第 k 段光纤引入的相移, τ_s 为光纤链路总时延。信号 E_2 的上下边带分别引入了 φ_s 和 $-\varphi_s$ 的相位波动。将 V_2 调

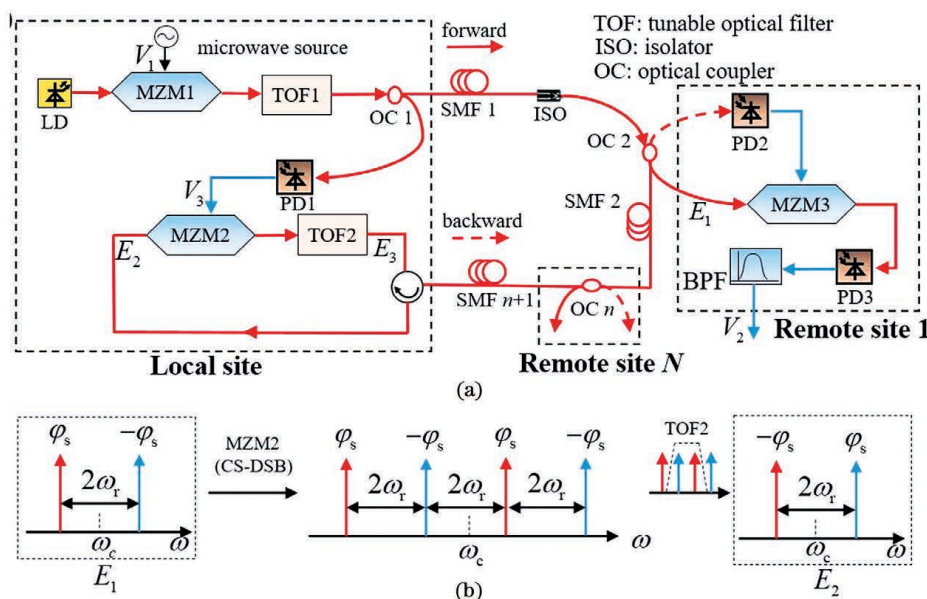


图 7 基于相位共轭原理的光纤频率同步网。(a) 原理图; (b) 相位共轭的光谱演化

Fig. 7 Fiber-optic frequency synchronization network based on phase conjugation. (a) Schematic diagram; (b) spectrum evolution of the phase conjugation

制为 E_2 , 产生 4 个一阶光边带, 通过光滤波以后, 得到 E_2 的相位共轭信号 E_3 , 表达式为

$$E_3 \propto \exp[j\omega_c(t - \tau_s)] \cdot \cos(\omega_r t + \varphi_s + \varphi_r). \quad (4)$$

将 E_3 沿原路径传回至远端站, 经光电转换后, 经偏置在正交点的 MZM3 调制前向传输的光信号 E_1 , 再经过 PD3 探测, 由带通滤波器(BPF)可得

$$V_3 \propto \cos[4(\omega_r t + \varphi_r)]. \quad (5)$$

得到的接收信号 V_3 为本地端参考频率信号的四倍

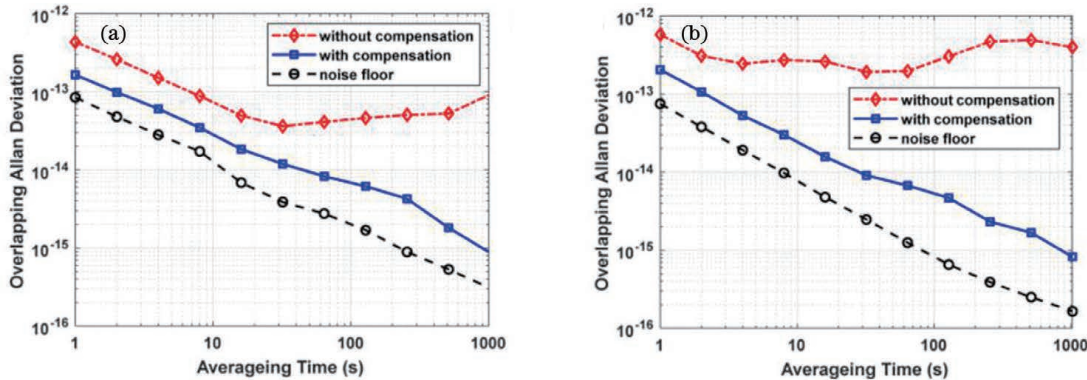


图 8 频率同步实验结果^[53]。(a) 远端站由两卷 10 km 单模光纤盘连接; (b) 远端站由一卷 5 km 和一卷 15 km 单模光纤盘连接

Fig. 8 Frequency synchronization experimental results^[53]. (a) Remote station connected by two 10 km SMF spools;
(b) remote station connected by a 5 km SMF spool and a 15 km SMF spool

基于时-频转换测量(TFDT)的光纤双向时间传递技术如图 9 所示。中心站和远端站分别通过数字频率合成器(DDS)产生周期啁啾脉冲, 经电光调

制后在 SMF1 上双向传递。随后, 两端通过时-频转换测量获得双向传输时延, 其原理如图 9(b)所示: 通过啁啾混频和时频变换分析, 可将时延 τ 转换为

实验中, 将本地站和远端站通过两卷总距离为 20 km 的单模光纤盘连接, 用于测试所提方案的同步性能, 得到如图 8 所示的实验结果^[53]。未经补偿的 10 GHz 信号频率稳定度恶化严重, 而补偿之后的 20 GHz 信号的长期频率稳定度被提高到 8.5×10^{-16} @ 1000 s。该方案实现了频率信号高稳定传输。

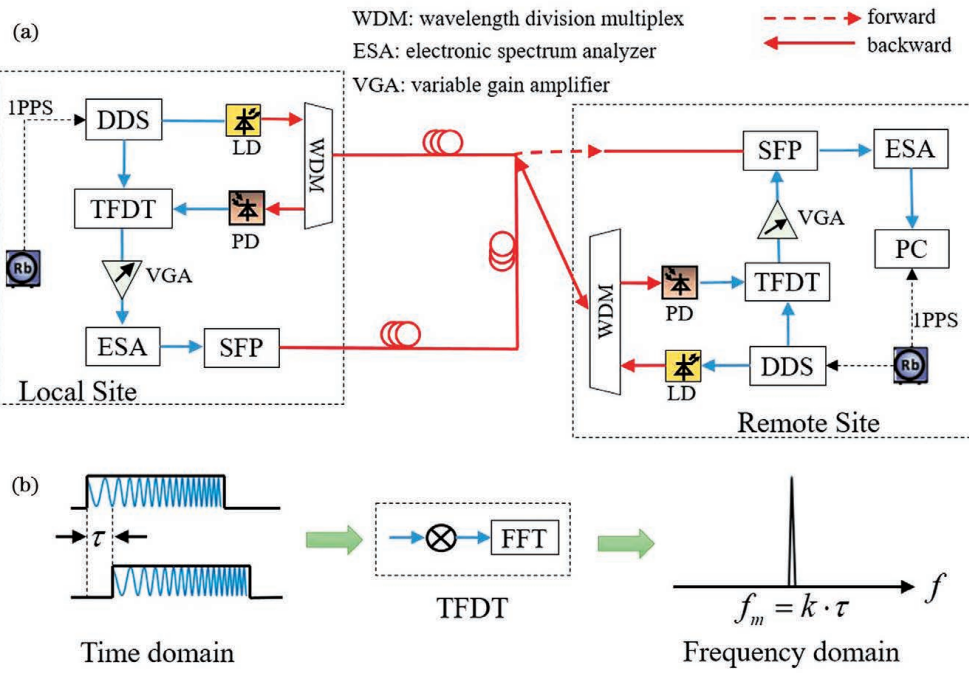


图 9 基于时频转换测量的光纤时间同步网络。(a) 原理图;(b) 时频转换测量原理

Fig. 9 Fiber-optic time synchronization network based on TFDT. (a) Scheme diagram; (b) principle of TFDT

差拍频率 f_m 进行测量。获取双向传输时延以后, 中心站通过光收发模块(SFP)将时延波动经 SMF2 传至远端站, 由 SFP 解调出时延信息传送给处理控制单元(PC), 并与远端站测量的时延作比对, 消除光纤链路时延抖动, 调整时钟, 完成时间同步。

实验中, 将中心站与远端站通过一段长为 1.7 km 的 SMF 和一段长为 4.2 km 的 SMF 连接。

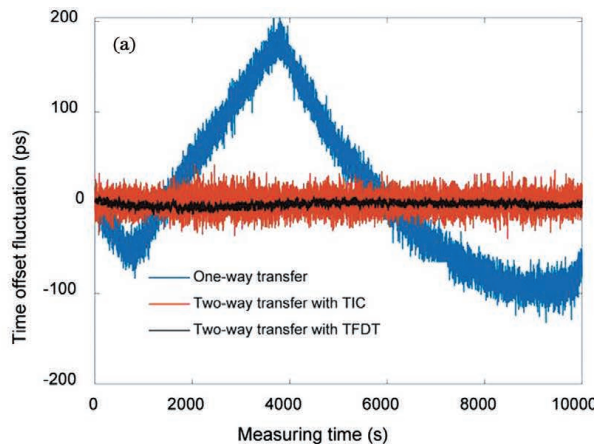


图 10 时间同步实验结果^[54]。(a)不同传递方式下两站时间差波动;

Fig. 10 Time synchronization experimental results^[54]. (a) Time difference fluctuation between the local site and the remote site in different time transfer ways; (b) time stabilities obtained in different time transfer ways

全光相位共轭的光纤频率稳相传输环形网结合双向时间传递方案形成的微波光子时频同步网络如图 11 所示。中心站用原子钟的 10 MHz 频率信号

啁啾脉冲信号起止频率分别为 4 GHz 和 6 GHz, 脉冲宽度为 50 μ s, 周期为 1 ms。实验比较了本地站与远端站之间通过单向传输、基于计数器(TIC)双向时间传输和基于 TFDT 双向时间传输三种情况。基于 TFDT 的双向时间传递技术^[54]可将时间差波动减小到 5.6 ps, 如图 10(a)所示; 可使时间偏差(TDEV)达到 0.36 ps@10000 s, 如图 10(b)所示。

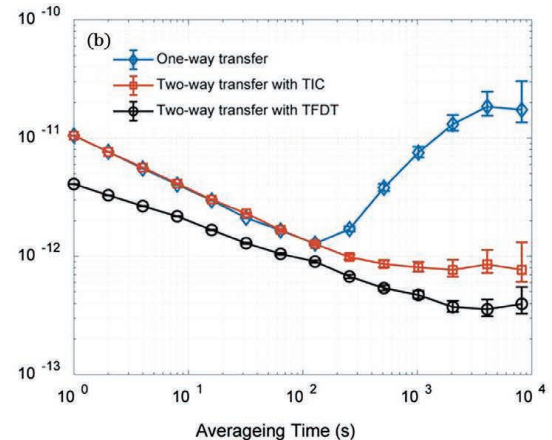


图 10 时间同步实验结果^[54]。(b)不同传递方式的时间稳定性

锁定微波源, 产生高稳定微波参考信号。在远端站, 接收到的微波信号通过分频和锁相环(PLL)后产生 10 MHz 频率参考信号, 同步远端站时钟。

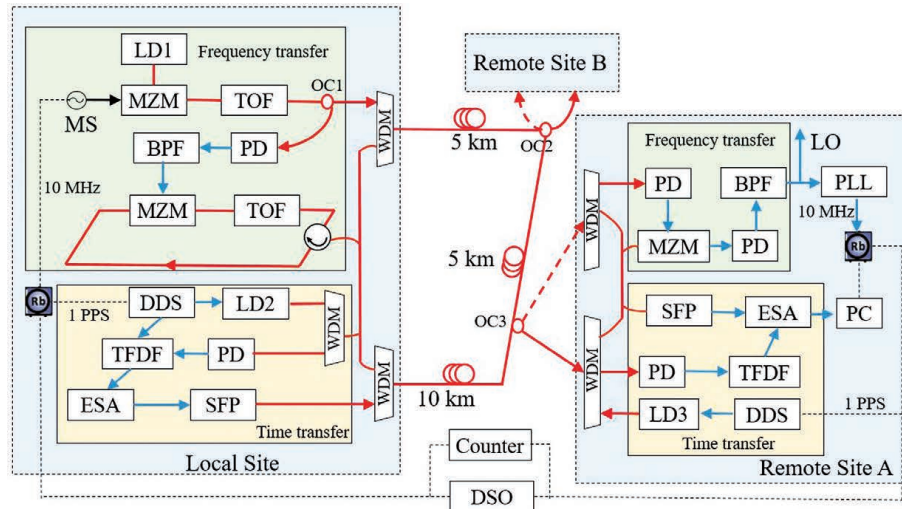


图 11 微波光子时频同步网络实验系统

Fig. 11 Experimental setup of the microwave photonic time-frequency synchronization network

该时频同步环网的时频信号的时延波动分别为 1.6 ps 和 8.9 ps, 如图 12(a)所示; 两个站点的频率稳定性分别为 5.0×10^{-16} @1000 s 和 7.2×10^{-16} @

1000 s, 如图 12(b)所示; 两个站点的 TDEV 分别为 0.5 ps@1000 s 和 0.8 ps@1000 s, 如图 12(c)所示。这个结果满足了典型波段全相参的需求。

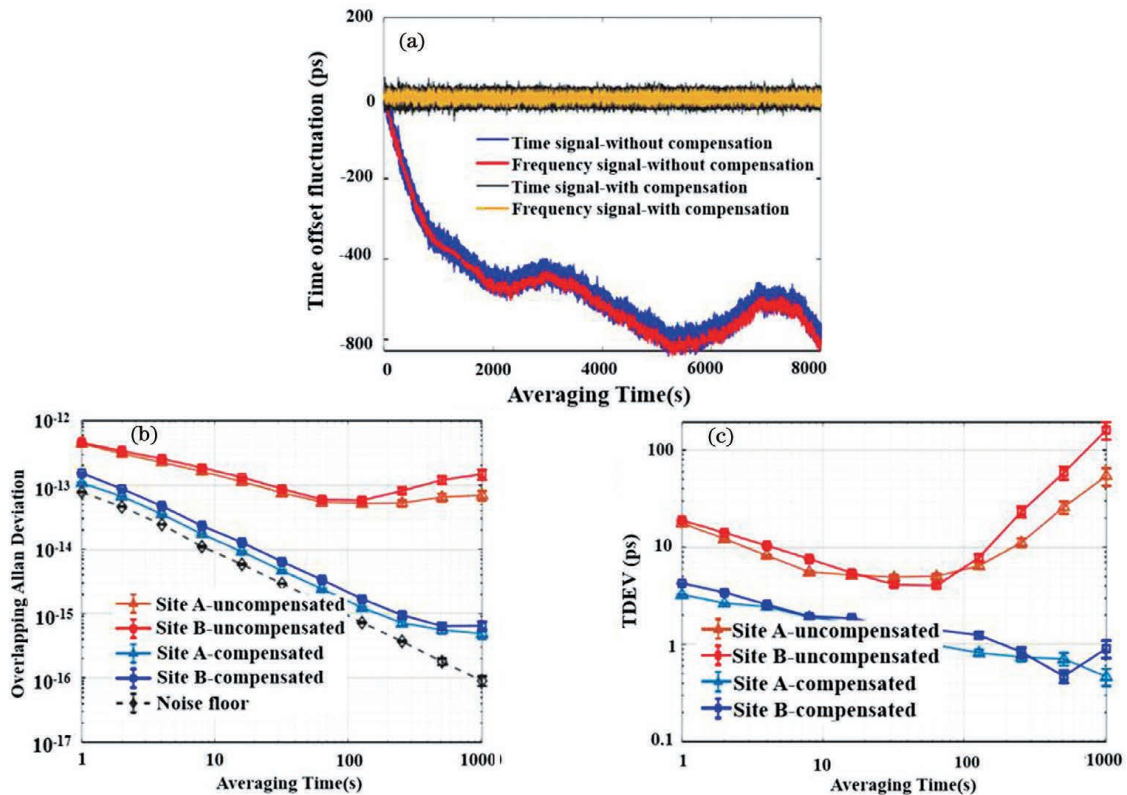


图 12 时频同步实验结果^[55]。(a)两站时频信号的时间差波动;(b)远端站的频率稳定度;(c)远端站的时间稳定度

Fig. 12 Time-frequency synchronization experimental results^[55]. (a) Measured time difference fluctuation of time-frequency signal between the local site and remote sites; (b) frequency stabilities of remote sites; (c) time stabilities of remote sites

3 分布式相参成像雷达实验

本课题组在前述关键技术的支持下,搭建了基于微波光子学原理的分布相参 X 波段、2 发 2 收、带宽为 4 GHz 的成像雷达实验系统,并分别基于静

态和动态光纤时频同步网实现了高分辨率、高信噪比成像。该系统不同于现有的、主要采用电子设备搭建的分布式相参雷达实验系统。图 13 为基于静态光纤时频同步网的分布式相参成像雷达实验系统。

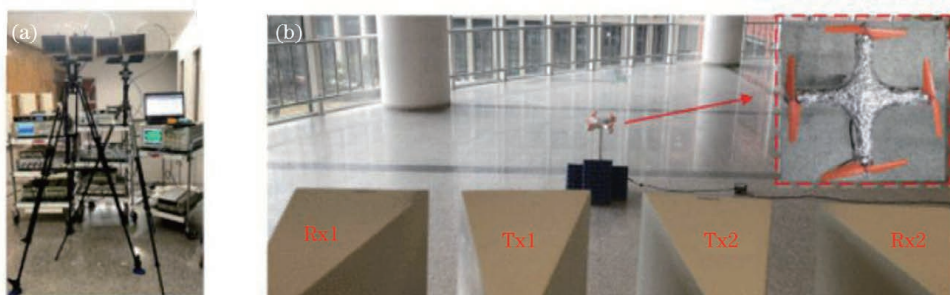


图 13 实验场景照片。(a)雷达发射机照片;(b)天线与目标照片

Fig. 13 Photographs of the experimental scene. (a) Photograph of the radar transceiver; (b) photograph of the antennas and the target

实验测得:接收相参情况下的信噪比增益最高为 5.98 dB,全相参情况下的信噪比增益最高为 8.6 dB。

对小型无人机的转台成像结果如图 14 所示,实验得到的距离向和方位向的分辨率分别为 3.4 cm 和 4.3 cm。图 14(a)和图 14(c)为两部雷达独自成像的结果,无人机的信号几乎淹没在噪声中。

图 14(b)和图 14(d)为两部雷达在发射相参情况下的成像结果,可以看到由于信噪比有所改善,无人机的像相对清晰。图 14(e)为全相参情况,其信噪比最高,成像最为清晰。

基于动态光纤时频同步环网的分布相参雷达的实验系统与场景如图 15 所示。

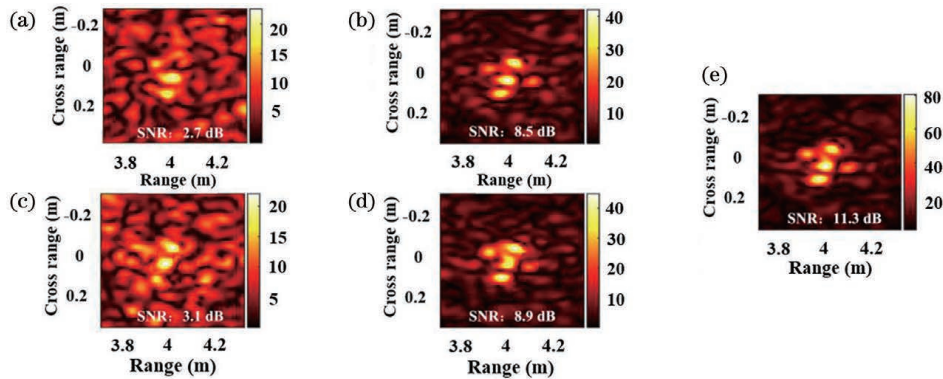


图 14 转台目标逆合成孔径雷达(ISAR)成像结果^[56]。(a)(c)雷达 1 和 2 的单发单收模式;(b)(d)雷达 1 和 2 的发射相参模式;(e)全相参模式

Fig. 14 ISAR imaging results of rotation platform^[56]. (a)(c) Monostatic mode of radar 1 and radar 2; (b)(d) coherence-on-transmit mode of radar 1 and radar 2; (e) full coherence mode

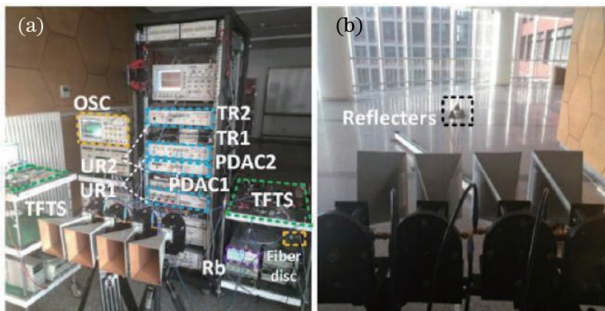


图 15 实验系统与实验场景^[57]。(a)实验系统;(b)实验场景

Fig. 15 Experimental setup and experimental scene^[57].

(a) Experiment setup;(b) experimental scene

实验测量了相参信噪比增益。发射相参可使两部雷达分别获得 5.69 dB 和 5.34 dB 的信噪比增益;

全相参情况下,两单元雷达分别获得了 8.1 dB 和 7.9 dB 的信噪比增益。

实验比较了单发单收、发射相参和全相参三种模式下三个角反射器的成像效果,结果如图 16 所示。可以看到:当单部雷达成像信噪比较低的时候,无法对三个目标进行清晰成像,如图 16(a)所示;发射相参可使两单元雷达各自获得一定的信噪比增益,距离目标较近的像的信噪比高,距离目标较远的像的信噪比相对弱一些,如图 16(b)所示;在全相参模式下,两单元雷达可获得更高的信噪比增益,三个角反射器目标可清晰分辨,如图 16(c)所示。该实验没有采取消除栅瓣的措施,因此结果中存在栅瓣的影响。

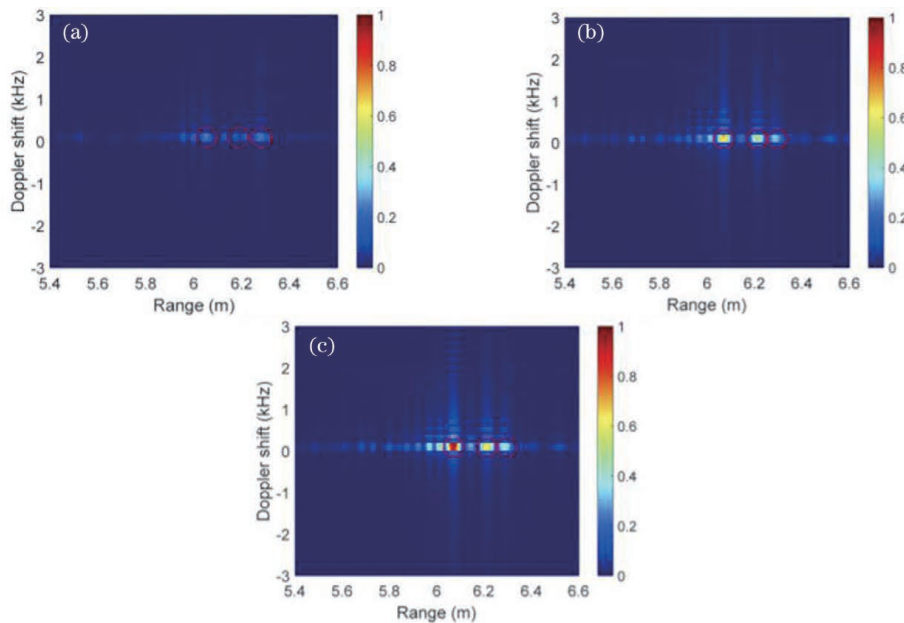


图 16 不同模式下反射器成像结果^[57]。(a)单发单收模式;(b)发射相参模式;(c)全相参模式

Fig. 16 Imaging results of reflectors in different modes^[57]. (a) Monostatic mode; (b) coherence-on-transmit mode; (c) full coherence mode

4 结 论

清华大学在分数域光学非线性调控、光子微波相位共轭信号处理、灵活波形产生等方面取得系列成果,研制了波形可重构的宽带波形发射端机、基于光子分数傅里叶的宽带信号接收前端,实现了高精度时频环网,最终构建了两种X波段、带宽为4 GHz的分布式微波光子相参成像雷达实验系统。基于静态光纤时频同步网的分布相参雷达在转台目标成像实验中获得了3.4 cm的距离向分辨率和4.3 cm的方位向分辨率,在全相参模式下最高获得8.6 dB信噪比增益;基于动态光纤时频同步网的分布相参雷达最高获得8.1 dB全相参信噪比增益。两种系统均实现了对弱小目标的高分辨率、高精度成像。

参 考 文 献

- [1] Coutts S, Cuomo K, McHarg J, et al. Distributed coherent aperture measurements for next generation BMD radar[C]//Fourth IEEE Workshop on Sensor Array and Multichannel Processing, 2006, July 12-14, 2006, Waltham, MA, USA. New York: IEEE Press, 2006: 390-393.
- [2] MIT Lincoln Laboratory. MIT Lincoln Laboratory 2008 annual report[EB/OL]. [2021-02-25]. <http://www.ll.mit.edu>.
- [3] Zhang Y T, Huang Z Z. A new system radar: distributed aperture coherence-synthesizing radar[J]. Fire Control Radar Technology, 2014, 43(2): 43-47. 张亚婷, 黄志忠. 新体制雷达—分布式孔径相参合成雷达[J]. 火控雷达技术, 2014, 43(2): 43-47.
- [4] Gao H W, Cao Z, Wen S L, et al. Study on distributed aperture coherence-synthesizing radar with several experiment results[C]//Proceedings of 2011 IEEE CIE International Conference on Radar, October 24-27, 2011, Chengdu, China. New York: IEEE Press, 2011: 84-86.
- [5] Cao Z, Chai Z H, Gao H W, et al. Technology and tests on distributed aperture coherence-synthesizing radar [J]. Modern Defence Technology, 2012, 40(4): 1-11. 曹哲, 柴振海, 高红卫, 等. 分布式阵列相参合成雷达技术研究与试验[J]. 现代防御技术, 2012, 40(4): 1-11.
- [6] Lu Y B, Gao H W, Zhou B L. Distributed aperture coherence-synthetic radar technology[J]. Journal of Radars, 2017, 6(1): 55-64. 鲁耀兵, 高红卫, 周宝亮. 分布式孔径相参合成雷达技术[J]. 雷达学报, 2017, 6(1): 55-64.
- [7] Zhou B L, Zhou D M, Gao H W, et al. Research on the distributed aperture coherence-synthetic radar system design and experiment[J]. Modern Defence Technology, 2018, 46(3): 112-119.
- [8] Zhou B L, Zhou D M, Gao H W, et al. Research on the distributed aperture coherence-synthetic radar system design and experiment[J]. Modern Defence Technology, 2018, 46(3): 112-119.
- [9] Vankka J, Halonen K. Direct digital synthesizer [M]//The Springer international series in engineering and computer science. Boston: Springer, 2001, 614: 8-17.
- [10] Robertson D A, Cassidy S L, Bolton D R. Nonlinearity and phase noise effects in 340 GHz 3D imaging radar[J]. Proceedings of SPIE, 2013, 8715: 87150M.
- [11] Jiang Z. Towards a TWSTFT network time transfer [J]. Metrologia, 2008, 45(6): S6-S11.
- [12] Bauch A, Achkar J, Bize S, et al. Comparison between frequency standards in Europe and the USA at the 10^{-15} uncertainty level[J]. Metrologia, 2006, 43(1): 109-120.
- [13] Yao J P. Microwave photonics [J]. Journal of Lightwave Technology, 2009, 27(3): 314-335.
- [14] Khilo A, Spector S J, Grein M E, et al. Photonic ADC: overcoming the bottleneck of electronic jitter [J]. Optics Express, 2012, 20(4): 4454-4469.
- [15] Walden R H. Analog-to-digital conversion in the early twenty-first century[J]. Wiley Encyclopedia of Computer Science and Engineering, 2008: ecse014.
- [16] Ridgway R W, Dohrman C L, Conway J A. Microwave photonics programs at DARPA [J]. Journal of Lightwave Technology, 2014, 32(20): 3428-3439.
- [17] Sliwczynski L, Krehlik P. Multipoint joint time and frequency dissemination in delay-stabilized fiber optic links[J]. IEEE Transactions on Ultrasonics, Ferroelectrics, and Frequency Control, 2015, 62(3): 412-420.
- [18] Li Y H, Rashidinejad A, Wun J M, et al. Photonic generation of W-band arbitrary waveforms with high time-bandwidth products enabling 3.9 mm range resolution[J]. Optica, 2014, 1(6): 446-454.
- [19] Rashidinejad A, Weiner A M. Photonic radio-frequency arbitrary waveform generation with maximal time-bandwidth product capability[J]. Journal of Lightwave Technology, 2014, 32(20):

- 3383-3393.
- [20] Zhang F Z, Guo Q S, Wang Z Q, et al. Photonics-based broadband radar for high-resolution and real-time inverse synthetic aperture imaging [J]. Optics Express, 2017, 25(14): 16274-16281.
- [21] Yao Y, Zhang F Z, Zhang Y, et al. Demonstration of ultra-high-resolution photonics-based Kaband inverse synthetic aperture radar imaging [C] // 2018 Optical Fiber Communications Conference and Exposition (OFC), March 11-15, 2018, San Diego, CA, USA. New York: IEEE Press, 2018: 1-3.
- [22] Simpson T B, Liu J M, Huang K F, et al. Nonlinear dynamics induced by external optical injection in semiconductor lasers [J]. Quantum and Semiclassical Optics: Journal of the European Optical Society Part B, 1997, 9(5): 765-784.
- [23] Zhou P, Zhang F Z, Guo Q S, et al. Reconfigurable radar waveform generation based on an optically injected semiconductor laser [J]. IEEE Journal of Selected Topics in Quantum Electronics, 2017, 23 (6): 1-9.
- [24] Zhang B W, Zhu D, Zhou P, et al. Tunable triangular frequency modulated microwave waveform generation with improved linearity using an optically injected semiconductor laser [J]. Applied Optics, 2019, 58(20): 5479-5485.
- [25] Kanno A, Kawanishi T. Broadband frequency-modulated continuous-wave signal generation by optical modulation technique [J]. Journal of Lightwave Technology, 2014, 32(20): 3566-3572.
- [26] Guo Q S, Zhang F Z, Zhou P, et al. Dual-band LFM signal generation by optical frequency quadrupling and polarization multiplexing [J]. IEEE Photonics Technology Letters, 2017, 29(16): 1320-1323.
- [27] Liao J X, Chen B Y, Li S Y, et al. Novel photonic radio-frequency arbitrary waveform generation based on photonic digital-to-analog conversion with pulse carving [C] // 2015 Conference on Lasers and Electro-Optics (CLEO), May 10-15, 2015, San Jose, CA, USA. New York: IEEE Press, 2015: 1-2.
- [28] Xiao X D, Li S Y, Peng S W, et al. Photonics-based wideband distributed coherent aperture radar system [J]. Optics Express, 2018, 26(26): 33783-33796.
- [29] Chou J, Conway J A, Seffler G A, et al. Photonic bandwidth compression front end for digital oscilloscopes [J]. Journal of Lightwave Technology, 2009, 27(22): 5073-5077.
- [30] Wong J H, Lam H Q, Li R M, et al. Photonic time-stretched analog-to-digital converter amenable to continuous-time operation based on polarization modulation with balanced detection scheme [J]. Journal of Lightwave Technology, 2011, 29 (20): 3099-3106.
- [31] Wang W S, Davis R L, Jung T J, et al. Characterization of a coherent optical RF channelizer based on a diffraction grating [J]. IEEE Transactions on Microwave Theory and Techniques, 2001, 49 (10): 1996-2001.
- [32] Xie X X, Dai Y T, Xu K, et al. Broadband photonic RF channelization based on coherent optical frequency combs and I/Q demodulators [J]. IEEE Photonics Journal, 2012, 4(4): 1196-1202.
- [33] Li T. Research on wideband acquisition and processing for digital electronic reconnaissance receiver [D]. Changsha: National University of Defense Technology, 2018.
- 李涛. 数字化电子侦察接收机宽带侦收与处理技术研究[D]. 长沙: 国防科技大学, 2018.
- [34] Guo Q. Research on optical signal processing for analog-to-information conversion [D]. Beijing: Tsinghua University, 2018.
- 郭强. 面向模拟信息转换的光信号处理研究 [D]. 北京: 清华大学, 2018.
- [35] Li P. Realization and research of photonic-assisted compressive sampling systems [D]. Beijing: Tsinghua University, 2017.
- 李佩. 基于光子辅助的压缩采样系统实现及性能研究 [D]. 北京: 清华大学, 2017.
- [36] Peng S W, Li S Y, Xue X X, et al. High-resolution W-band ISAR imaging system utilizing a logic-operation-based photonic digital-to-analog converter [J]. Optics Express, 2018, 26(2): 1978-1987.
- [37] Li R M, Li W Z, Ding M L, et al. Demonstration of a microwave photonic synthetic aperture radar based on photonic-assisted signal generation and stretch processing [J]. Optics Express, 2017, 25 (13): 14334-14340.
- [38] Ye X W, Zhang F Z, Yang Y, et al. Photonics-based radar with balanced I/Q de-chirping for interference-suppressed high-resolution detection and imaging [J]. Photonics Research, 2019, 7(3): 265-272.
- [39] Han G Y, Li S Y, Xue X X, et al. Photonic fractional Fourier transformer for chirp radar with ghost target elimination [J]. Optics Letters, 2020, 45 (15): 4228-4231.
- [40] Wei K K. Research on generation of microwave signal and bias control technology based on external modulator [D]. Xi'an: Xidian University, 2019.
- 魏孔坤. 基于电光调制器的微波信号生成及偏压控制技术研究 [D]. 西安: 西安电子科技大学, 2019.
- [41] Lopez O, Amy-Klein A, Lours M, et al. High-resolution microwave frequency dissemination on an

- 86-km urban optical link [J]. Applied Physics B, 2010, 98(4): 723-727.
- [42] Zhang A X, Dai Y T, Yin F F, et al. Phase stabilized downlink transmission for wideband radio frequency signal via optical fiber link [J]. Optics Express, 2014, 22(18): 21560-21566.
- [43] Ning B, Hou D, Zheng T L, et al. Hybrid analog-digital fiber-based radio-frequency signal distribution [J]. IEEE Photonics Technology Letters, 2013, 25(16): 1551-1554.
- [44] Shen J G, Wu G L, Hu L, et al. Active phase drift cancellation for optic-fiber frequency transfer using a photonic radio-frequency phase shifter [J]. Optics Letters, 2014, 39(8): 2346-2349.
- [45] Wang X C. The research on the time and frequency signal transmission via optical fiber with high stability [D]. Shanghai: Shanghai Jiao Tong University, 2019.
- 王小成. 时间和频率信号的光纤稳定传输技术研究 [D]. 上海:上海交通大学, 2019.
- [46] Li D, Hou D, Hu E, et al. Phase conjugation frequency dissemination based on harmonics of optical comb at 10^{-17} instability level [J]. Optics Letters, 2014, 39(17): 5058-5061.
- [47] Li W, Wang W T, Sun W H, et al. Stable radio-frequency phase distribution over optical fiber by phase-drift auto-cancellation [J]. Optics Letters, 2014, 39(15): 4294-4296.
- [48] Yin F F, Zhang A X, Dai Y T, et al. Phase-conjugation-based fast RF phase stabilization for fiber delivery [J]. Optics Express, 2014, 22(1): 878-884.
- [49] Smotlacha V, Kuna A, Mache W. Time transfer using fiber links [C] // EFTF-2010 24th European Frequency and Time Forum, April 13-16, 2010, Noordwijk, Netherlands. New York: IEEE Press, 2010: 1-8.
- [50] Yin F F, Wu Z L, Dai Y T, et al. Stable fiber-optic time transfer by active radio frequency phase locking [J]. Optics Letters, 2014, 39(10): 3054-3057.
- [51] Wu G L, Hu L, Zhang H, et al. High-precision two-way optic-fiber time transfer using an improved time code [J]. Review of Scientific Instruments, 2014, 85(11): 114701.
- [52] Abuduweili A, Chen X, Shang J M, et al. Sub-picosecond resolution time-offset measurement over fiber link with asynchronous optical sampling [C] // CLEO: Science and Innovations 2018, May 13-18, 2018, San Jose, California. Washington, D. C.: OSA, 2018: SM1L-2.
- [53] Wang H J, Xue X X, Li S Y, et al. All-optical arbitrary-point stable quadruple frequency dissemination with photonic microwave phase conjugation [J]. IEEE Photonics Journal, 2018, 10(4): 1-8.
- [54] Wang H J, Li S Y, Xue X X, et al. High-precision fiber-optic two-way time transfer network with time-frequency transform measurement [J]. Optics Communications, 2020, 477: 126342.
- [55] Wang H J. Research on microwave photonic time frequency synchronization technologies with applications in distributed coherent radar [D]. Beijing: Tsinghua University, 2020.
- 王豪杰. 微波光子时频同步技术研究及在分布式相参雷达中的应用 [D]. 北京: 清华大学, 2020.
- [56] Xiao X D, Li S Y, Xue X X, et al. Photonics-assisted broadband distributed coherent aperture radar for high-precision imaging of dim-small targets [J]. IEEE Photonics Journal, 2019, 11(5): 1-9.
- [57] Wang H J, Li S Y, Xue X X, et al. Distributed coherent microwave photonic radar with a high-precision fiber-optic time and frequency network [J]. Optics Express, 2020, 28(21): 31241-31252.

High-Frequency Broadband-Distributed Coherent-Aperture Microwave Photonic Imaging Radar

Xing Yunlu, Li Shangyuan, Xue Xiaoxiao, Zheng Xiaoping^{*}

Department of Electronic Engineering, Beijing National Research Center for Information Science and Technology,
Tsinghua University, Beijing 100084, China

Abstract

Significance As targets become increasingly complicated, image detection with high sensitivity, high resolution, and high precision has become essential. However, owing to their high cost and large size, monostatic radars fail to meet the abovementioned requirements. To overcome this problem, we propose a distributed coherent-aperture-

imaging radar (DCAIR). DCAIR is a novel radar system that uses multiple spatially dispersed small-aperture unit radars for cooperative detection and imaging. By employing the signal-level coherent fusion of the unit radars, the DCAIR obtains target images with high signal-to-noise ratios (SNRs). Thus, it is an important means to deal with long-range, low radar cross sections (RCS), or small threats. Additionally, DCAIR has many advantages such as flexibility, high survivability, low cost, and strong maintainability, making DCAIR an important development in the direction of imaging radars. Further improving the detecting resolution requires DCAIR to generate and process high-frequency broadband signals. However, traditional DCAIR realized using purely electronic technologies suffers severely from the “electronic bottlenecks”, making it difficult to generate and process high-frequency broadband radar signals directly. Moreover, conventional time and frequency synchronization technologies fail to strike a balance among the transmission distance, stability performance, and synchronization precision. Microwave photonics has been considered a promising solution to these bottlenecks. Because of the broad bandwidth, flat response, low loss transmission, and multidimensional multiplexing of photonics devices, microwave photonic technologies have merits in high-frequency broadband signal generation, transmission, and processing. Combined with microwave photonic technologies, DCAIR exhibits better performance in terms of range resolution, velocity resolution, angular resolution, and SNR gain. With the funding of major programs of the National Natural Science Foundation of China, many achievements have been made. This paper highlights the achievements of DCAIR based on microwave photonic technologies proposed by researchers at Tsinghua University.

Progress In this paper, the international developing status of the three key modules is briefly reviewed, including generation of a dynamic reconfigurable waveform, optical fractional Fourier domain receiver front-end, and high-precision fiber-optic time-frequency synchronization network (OTFSN), and the the achievements funded by the major program of the National Natural Science Foundation of China are highlighted. From these achievements, the first experimental X-band distributed coherent broadband imaging radar system using microwave photonics was built and the staged experimental results were obtained. To generate multichannel orthogonal waveforms and achieve dynamic switching to coherent waveforms, a generation method for dynamic reconfigurable radar waveform using photonics-based broadband is proposed. We use the phase-coded linear frequency modulated waveform (PCLFMW) as the orthogonal waveform and the linear frequency modulated waveform (LFMW) as the coherent waveform. Here, two PCLFMWs in X-band with a bandwidth of 3.5 GHz are generated and the orthogonality between the waveforms reaches about 29 dB (Fig. 3). The proposed scheme achieves arbitrary generation and dynamic reconfiguration of the waveform. Furthermore, an optical FrFD receiver front-end is proposed to eliminate ghost targets produced by multiple echoes that are overlapped in both the time and frequency domains. The received broadband LFMW echo signals are projected on the optimal fractional Fourier domain formed using the photonic rotation of the time-frequency plane. By controlling the fractional Fourier transform spectrum, the proposed receiver front-end cancels ghost targets in multitarget circumstances. Experimental results show that the proposed receiver front-end can adapt to multiple noncooperative target environments and is immune to ghost targets under optimal working conditions (Fig. 6). An all-optical stable quadruple frequency dissemination scheme using photonic microwave phase conjugation is presented over a fiber-optic loop link. The relative frequency stability of 10^{-16} at 1000-s averaging time can be obtained at every remote site located at a 20-km fiber loop link (Fig. 8). Moreover, a fiber-optic two-way time transfer method based on the time-frequency domain transforms (TFDT) is proposed. The TFDT directly obtains the two-way transmission delay by chirp frequency mixing and time-frequency analysis. With the proposed method, the time offset fluctuation and TDEV can reach 5.6 and 0.36 ps at 10000 s, respectively (Fig. 10). Further, using the stable frequency transfer technology, a three-node time-frequency synchronization network over a 20-km fiber loop link is presented. At 1000-s averaging time, frequency stability levels reach 10^{-16} and time deviations reach 0.5 and 0.8 ps for two sites, respectively (Fig. 12). Two X-band two-unit microwave photonic DCAIRs based on the static and dynamic OTFSN are demonstrated. From the static OTFSN, the SNR gain ratio relative to the coherence-on-transmit mode is ~ 5.98 dB and that for the full coherence mode is ~ 8.6 dB. The range and cross-range resolution of 3.4 cm and 4.3 cm, respectively, are achieved in the experiment for rotating-target imaging (Fig. 14). From the dynamic OTFSN, the fully coherent SNR ratio gain can be increased by 8.1 and 7.9 dB, respectively, for the two-unit radars (Fig. 16). Thus, weak targets can be imaged and probed using the mutually coherent operation, while they are undetectable using the single radar.

Conclusions and Prospect This paper introduces the achievements of high-frequency broadband DCAIRs using microwave photonics technologies proposed by researchers of Tsinghua University. Combined with microwave

photonic technologies, DCAIR realizes high-resolution and high-precision imaging. The abovementioned achievements will promote the development of DCAIR. The microwave photonics-based DCAIR has a wide application potential in both civil and military fields.

Key words microwave photonics; distributed coherent aperture; radar; fiber-optic time-frequency synchronization network; fractional Fourier transform

OCIS codes 060.2360; 060.4250; 060.5625